



AGATA: mechanics and infrastructures

R. Smith¹, R. Menegazzo², C. Aufranc³, N. Bez², I. Burrows¹, M. Cahoreau⁴, G. Debras⁵, L. Gibelin⁴, A. Goasduff⁶, A. Grant¹, T. Joannem⁵, N. Karkour⁴, M. Karolak⁵, J. Kieffer⁵, A. Lotodé⁵, B. Million⁷, P. S. Morrall¹, L. Ramina², M. Rampazzo², A. Roger⁵, J. Simpson^{1,a}, N. Solenne⁵, O. Stézwowski³, S. Tzvetkov⁵, L. Zago^{6,8}, M. Zielińska⁵

¹ STFC Daresbury Laboratory, Daresbury, Warrington WA4 4AD, UK

² Istituto Nazionale di Fisica Nucleare (INFN), Sezione di Padova, Padova, Italy

³ Université Lyon, Université Claude Bernard Lyon 1, CNRS/IN2P3, IP2I, Lyon, France

⁴ IJC Lab, CNRS/IN2P3, Université Paris-Saclay, 91406 Orsay, France

⁵ Irfu, CEA, Université Paris-Saclay, 91191 Gif-sur-Yvette, France

⁶ Laboratori Nazionali di Legnaro, Istituto Nazionale di Fisica Nucleare (INFN), Legnaro, Italy

⁷ Istituto Nazionale di Fisica Nucleare (INFN), Sezione di Milano, Milano, Italy

⁸ Dipartimento di Fisica, Università di Padova, Padova, Italy

Received: 6 March 2023 / Accepted: 1 June 2023 / Published online: 20 July 2023

© The Author(s) 2023

Communicated by Nicolas Alamanos.

Abstract The successful operation of AGATA requires a complex mechanical support structure for the safe and reliable operation of the detectors. Three mechanical structures were designed for the scientific campaigns at LNL, GSI and GANIL, each accommodating an increasing number of detectors. The present phase of the project, to increase the number of detectors from 60 to 180 (the 4π spectrometer), required a new concept in mechanical support. The detectors also require a suite of associated instrumentation, infrastructures and good system design for their optimum performance. This includes the automatic liquid nitrogen filling system, high and low voltage power supplies, and a series of signal cables and distribution systems. A well-designed electromagnetic compatibility across all the sub-systems is essential. An additional requirement is an easily accessible database that records the status of the wide range of components utilised on the project. This article describes all aspects of the mechanics and infrastructures.

1 Introduction

The mechanical structure, detector support system (DSS) and associated infrastructures are essential for the safe and reliable operation of the AGATA spectrometer. The mechanics is based on an array of flanges that hold germanium (Ge) detectors in a structure that will ultimately hold 180 detectors (60 triple detector modules), in a 4π configuration. Three support structures were designed for the first

experimental campaigns at Laboratori Nazionali di Legnaro (LNL), GSI Helmholtzzentrum für Schwerionenforschung and Grand Accélérateur National d'Ions Lourds (GANIL). The structures supported an increasing numbers of detectors and were adapted to the specific requirements of each host laboratory. The new structure, which takes AGATA from 20 triple detector modules to 60, is based on a concept to hold each half of the full array from a support shaft that enables rotation of the flange array. The DSS and associated infrastructures, for the maintenance and operation of the detectors, consists of many sub-systems. These include the low voltage power supplies (LVPS) and high voltage power supplies (HVPS) for the detectors and control systems, the automatic liquid nitrogen (LN_2) filling system, the detector and service cable management system, cables, optical fibres, and detector patch boxes for noise filtering and signal distribution. A well designed earthing system and overall electromagnetic compatibility throughout all the sub-systems, including the mechanics, detectors and electronics, is essential for optimum performance. Details about all array components are maintained and shared within the AGATA collaboration using a dedicated database. The mechanics and all associated infrastructures for AGATA are described in Sects. 2 and 3, respectively.

^a e-mail: john.simpson@stfc.ac.uk (corresponding author)

2 The AGATA mechanics

2.1 Introduction

The AGATA mechanics provide a stable mechanical support system that holds the detectors in a precise location in a spherical geometry surrounding the target position. The structure has been modified for each of its host sites and adapted to local infrastructures and its coupling to various spectrometers. The structures incorporate rotation and translation for safe insertion and removal of the detector modules and access to the target chamber. The design of the structures has to take into account the LN₂ filling (autofill) system, LVPS, HVPS and cables from the detectors to the electronics. The structures designed for the first implementation at LNL [1,2] then subsequent campaigns at GSI [3] and GANIL [4], as the spectrometer gradually increased in the number of detectors to 60, will be discussed. The present phase of the project is to move towards a full 4π system of 180 detectors. The new design and implementation for this phase, which started operation at LNL in 2022, is discussed in detail.

2.2 The detector module

The basic concept of tracking requires that the Ge detectors to cover as much of the total solid angle as possible. GEANT4 [5] simulations were performed on many geometries [6] and concluded that the optimum configuration to cover 4π is a geodesic tiling of a sphere with 180 hexagons and 12 pentagons, see Fig. 1. The Ge detectors occupy the hexagon positions, whereas the pentagon openings provide a pathway for the beam pipe and locations to support the structure. Three detectors, of slightly different shapes, are grouped together and mounted in a “triple” cryostat, which is used to keep the detectors at LN₂ temperature and house the 111 preamplifiers for each signal [7]. This AGATA Triple Cluster (ATC) [8] and associated mechanics is referred to as a triple detector module, or simply module, in this section. The key task of the mechanical design is to mount these identical modules in a frame as close as possible. The design aim was for a maximum of 0.5 mm clearance between the endcaps of adjacent modules.

2.3 The flange array

The mechanical structure comprises of two main elements: a spherical array to house the triple detector modules and a frame to support this array. There are two options for the mechanical design, a solid shell to house many modules as used in the GRETA design [9], or to have individual flanges for each module that lock together to form a single supporting structure. Due to the variety of spectrometers that AGATA is coupled to, some requiring rotation of the array, and the dif-

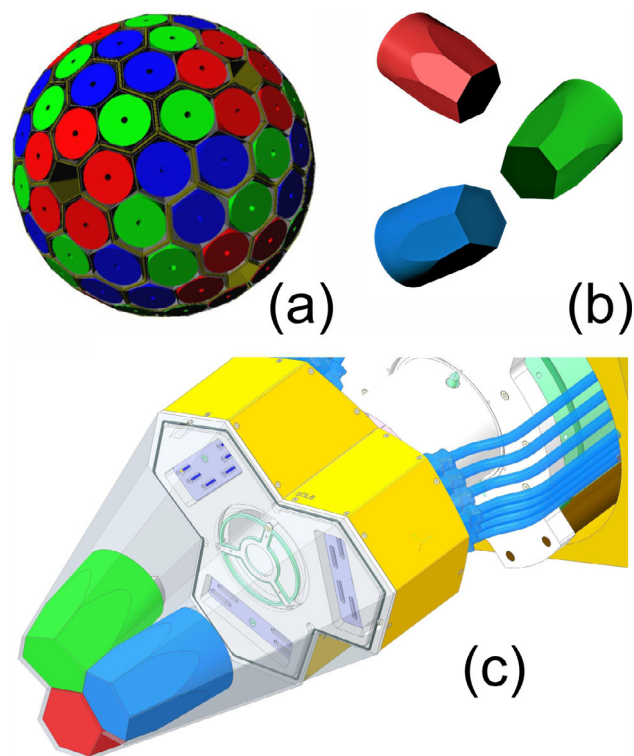


Fig. 1 CAD images of **a** tiling of a sphere with 180 detectors, **b** the three, slightly different, tapered hexagonal Ge crystals and **c** the AGATA triple cluster with the Ge crystals

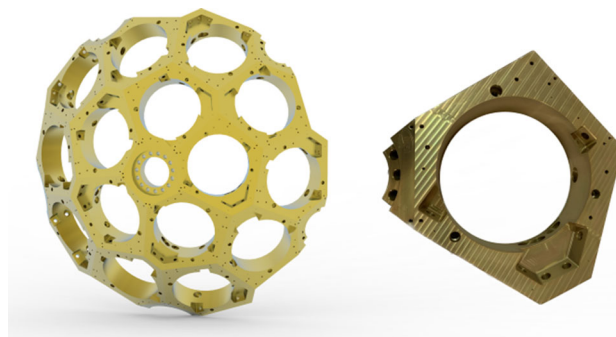


Fig. 2 CAD image of the 15 flange 1π array and a photograph of one flange. For scale the diameter of the spherical array of flanges is 1800 mm and the inner diameter of the bore in a flange is 325 mm

ferent number of detectors, it was decided to adopt a modular array design concept using individual flanges, see Fig. 2. The flanges are made from aluminium MIC-6™, a dimensionally stable material that is free from internal stresses. Each flange holds a triple detector module with the front face of the ATCs at a nominal distance of 230 mm from the target centre. The same flange design, with minor modifications, has been used in all of the AGATA structures.

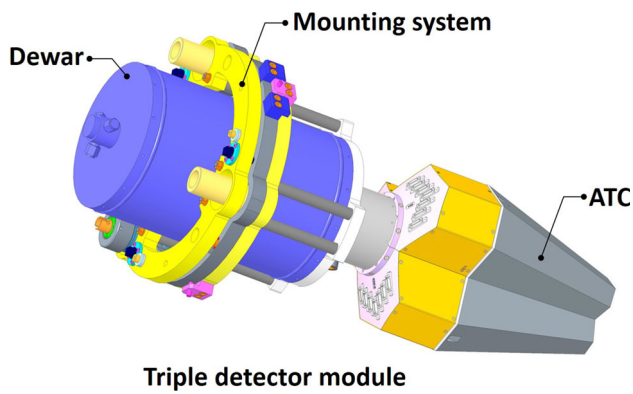


Fig. 3 CAD image of the triple detector module and its components

2.4 Detector mounting 2009–2021

An important aspect of the mechanical design is to provide a system for the careful insertion and removal of the triple detector modules into the flanges, see Fig. 3. In view of the module's weight, fragility, complex nature and high cost, careful handling and alignment is paramount to prevent damage. When inserted into the array, the module's endcaps form a closely-packed cluster with a nominal clearance of 0.5 mm between endcaps, so it is important to ensure that the modules begin their journey, down the insertion axis, on the correct path. Before they are lifted into the array, modules are placed into a setting jig and aligned to a nominal position with the aid of the detector's mounting system, see Fig. 4a. The mounting system is a kinematic adjustment mechanism that is located on the outside of the module. This comprises three rings that provide full 6 degrees of freedom of adjustment capability and provides ± 8 mm in horizontal planes, ± 10 mm vertically and an angular adjustment of ± 2 degrees with yaw and roll alignment achieved by differential adjustment between the three kinematic adjusters, see Fig. 3. This precise adjustment enables each module to correct positional errors introduced by machining accuracy limitations on all elements of the module, cantilevered load deflections and an accumulation of tolerances. The 80 kg weight of the module means that manual handling is not possible and mechanical assistance is required. Each module was raised into position using lifting features on the top and bottom of the dewar, see Fig. 4b. Positioning of the modules on the array was achieved by using three long precision sliding rods attached to the designated flange, one of which was threaded to help control the module's descent during insertion, see Fig. 4c.

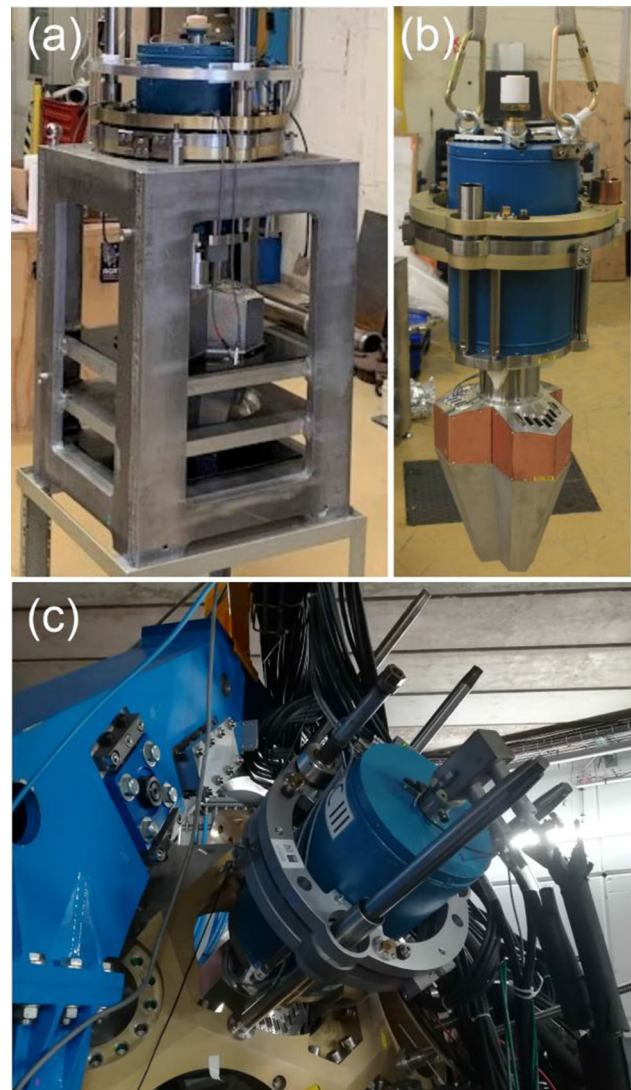


Fig. 4 **a** The setting jig, mounting system and rods. **b** An ATC being lifted for mounting and removal. **c** An ATC being located in the flange onto three long sliding rods

2.5 Installations for the campaigns at LNL, GSI and GANIL (2010–2021)

2.5.1 AGATA campaign at LNL 2010–2011

AGATA's first implementation with a 15-flange, 1π structure was at LNL, Italy, where it was commissioned in-beam in 2009 and its science campaign was from 2010 to 2011 [1,2].

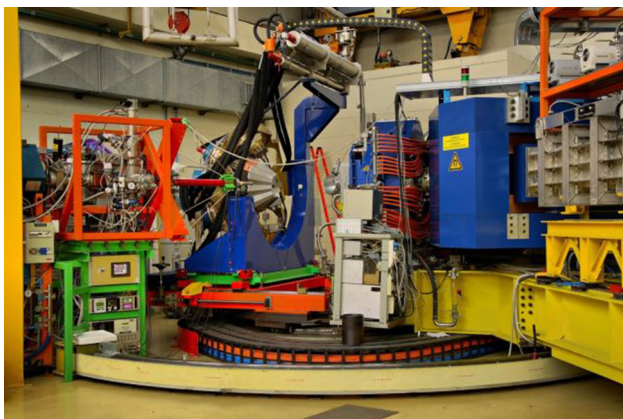


Fig. 5 The setup at LNL for the first campaign in 2009–2011

Its supporting structure was coupled to the PRISMA magnetic spectrometer [10] via a linear rail system, so that the target-to-detector distance could be altered and allow access to the reaction chamber in the centre, see Fig. 5. Both AGATA and PRISMA sat on a rotating platform that enabled them to rotate around the target as a single element. The 15-flange array was assembled and aligned using a combination of a portable coordinate measuring arm and a laser tracker before being mounted onto the main support structure. During the first campaign at LNL, five modules were mounted centrally on the flange array, see Fig. 5. The flange array was static in relation to the main support structure, therefore it was often challenging and time-consuming to lift and orientate the modules precisely to match their designated flange.

2.5.2 AGATA campaign at GSI 2012–2014

In 2012, AGATA moved from LNL to GSI, Germany, and located at the focal plane of the fragment separator. Complementary detectors including LYCCA [11], the HECTOR array [12] and Miniball detectors [13] were included in the setup [3]. The mechanics made allowances for the higher beam height (2000 mm compared with 1740 mm at LNL) with the beam passing through the centre of the array at 0 degrees, an increase in the number of modules from five to seven and further updates to accommodate extra triple detector module related services. A redesigned main support structure enabled the 1π array to be rotated, which allowed all modules to be inserted and removed horizontally, thus simplifying and speeding up the process. The support structure was mounted on existing linear rails from RISING [14] that ran perpendicular to the beam, so that the whole assembly could be split vertically in two sections, allowing access to the target position. Figure 6 shows a photograph of the split mechanical structure at GSI.

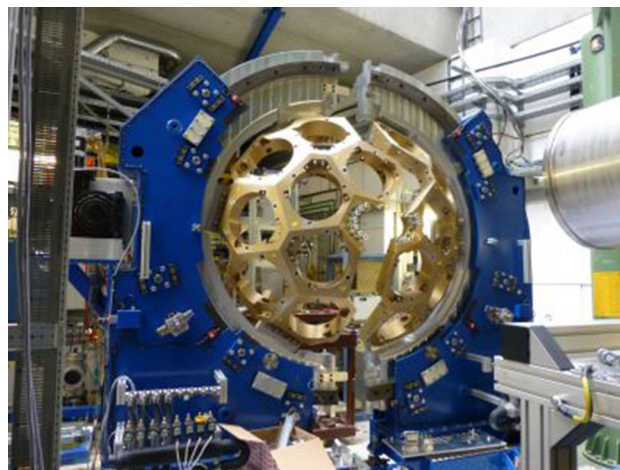


Fig. 6 The mechanical structure at GSI between 2012–2014

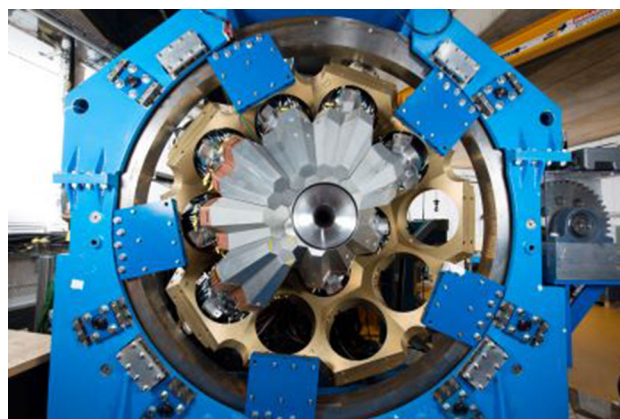


Fig. 7 AGATA at GANIL with 11 ATCs mounted (February 2017)

2.5.3 AGATA campaign at GANIL 2015–2021

In 2014, the AGATA 1π array was moved to GANIL, France and placed at the target position of the VAMOS++ spectrometer [15], and coupled to many other complementary detector systems [4]. In-beam commissioning took place in 2014 and the science campaign started in 2015. The 1750 mm beam height at GANIL was lower than at GSI, so the earlier supporting structure from GSI could not be reused. The basic design with the rotating array was replicated, see Fig. 7, with modifications to account for the reduced beam height and removal of its ability to split vertically perpendicular to the beam direction since this was not a requirement. The number of modules at GANIL increased from 7 to 15.

2.6 The mechanical structure as AGATA evolves to 4π

AGATA is now at a new phase with the aim to complete the 4π spectrometer of 180 detectors. The main design concept is to keep the same overall structure in each host laboratory and

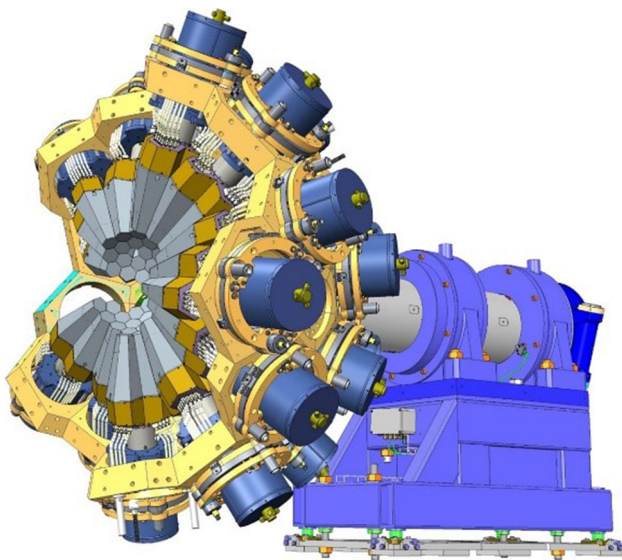


Fig. 8 CAD image of the 2π structure with the detector modules, flange array, support shaft and base frame

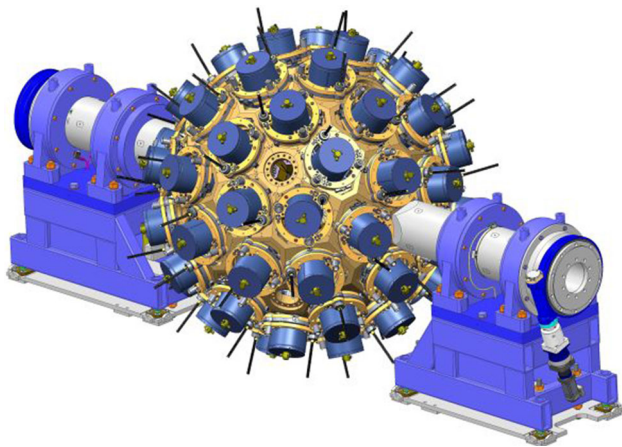


Fig. 9 CAD image of the future 4π structure

to reuse as many existing elements as possible. The design will continue to utilise modular flanges. However, to realise 4π a new holding system was required.

The general concept, shown in Fig. 8, is to support each half of the spherical array using a cantilever support shaft. The 30 flange hemi-spherical array accommodates 90 Ge detectors and connects to the shaft via its central pentagon. The shaft enables full rotation of the array, which facilitates module insertion and removal. Each half is mounted on a base frame to allow translational movement. This design takes inspiration from GRETA [9] in that it utilises a cantilevered support that couples with a second identical 2π system to create the full 4π geometry for future campaigns. A CAD image of the final 4π AGATA configuration is shown in Fig. 9.

The first campaign in this new phase is at LNL where a 2π system is located at the target position of the PRISMA

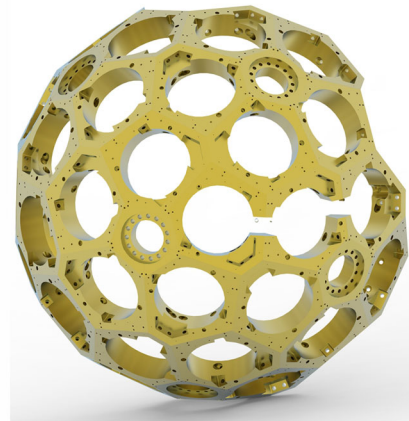
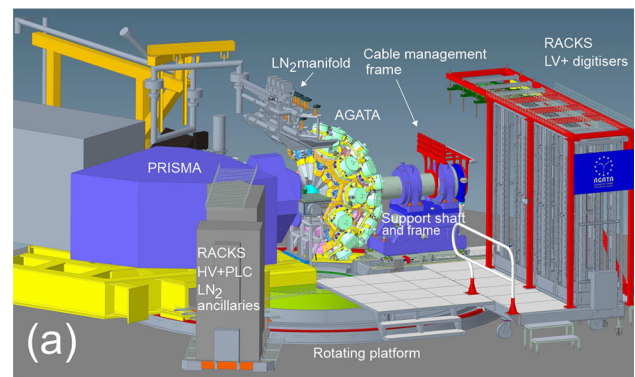


Fig. 10 **a** CAD image of the general layout at LNL indicating some key components. **b** The 30 flange 2π array, diameter 1800 mm, with three flanges slotted to accommodate rotation

spectrometer, see the general layout in Fig. 10a. A requirement is to accommodate the rotation of the PRISMA magnetic spectrometer over a large angle range with respect to the beam direction without breaking the vacuum in the beam line and target chamber. This results in the incoming beam pipe sweeping through the hemi-spherical flange array and hence a number of slotted flanges are required, see Fig. 10b. The support shaft has a central bore that allows the beam to pass through its central axis when AGATA is positioned at 180 degrees in relation to the beam direction. The control system limits the shaft's rotation to ± 85 degrees as this provides each one of the 30 modules with a horizontal insertion path whilst reducing the travel and lengths of the service cables routed to the modules. The base frame sits on a linear rail system that enables AGATA to have different target-to-detector distances and for access to the reaction chamber. In order to fit within the limited space constraints in the experimental hall, the LN_2 manifold is fixed directly on top of the 2π array, see Fig. 10a.

2.6.1 Flange array

In addition to the 30 mounting locations, the assembled 2π array has six pentagons, each with a 160 mm diameter central bore. In previous campaigns, this feature allows the beam to pass through the array and provided accurate reference features to mount flange alignment tools during the array's assembly. For the current LNL campaign, the central pentagon on the beam axis is used to locate and fix the array onto the support shaft. The flanges related to this one central pentagon have clearance holes instead of tapped holes to allow high-tensile fasteners to secure the array onto the support shaft. Three flanges on the horizontal beam plane have an 85 mm slot to allow the beam pipe at LNL to pass through the flanges between 20 and 110 degrees. In this configuration, the maximum number of modules is 27, as the slotted flanges currently cannot accommodate a standard module mounting system. In the previous set-ups, the 1π array was assembled before being lifted and secured to the main support structure, whereas now individual flanges are mounted sequentially on the shaft in order to utilise the shaft's alignment features and avoid issues with lifting a larger 2π array. The LN_2 manifold mounts directly to the internal faces of the upper flanges of the array, enabling it to rotate with the array and provide short feed lines from the distribution manifold to each module.

2.6.2 Support shaft

One of the design drivers to support the hemi-spherical array at a single location by a cantilevered shaft was that it optimises the surrounding space for installing and removing the modules, detector-related electronics and cryogenic services. Fifteen M20 high-tensile bolts secure the array to the 360 mm diameter support shaft via the array's central pentagon. The 1640 mm long shaft is machined from a single piece of 605M36T high-tensile steel with an 80 mm diameter bore through its centre to allow a beam pipe to pass through. To provide the desired rotary precision and stiffness, the pressed fit shaft is supported by two high-load spherical roller bearings, which are housed inside steel bearing housings that were cast specifically for AGATA. The shaft is rotated by a motor and gearbox-driven slew drive that is mounted directly to the shaft and end bearing housing.

2.6.3 Base frame

A fabricated steel support frame provides a stiff and stable base for mounting the heavy-duty bearings that support the cantilevered shaft and array.

The main alignment of the complete array is achieved via M56 fine-pitch adjusters on each corner of the base frame that allows ± 15 mm adjustment in horizontal planes, ± 20 mm vertically and an angular adjustment of ± 0.5 degrees. Yaw

and roll alignment is achieved by differential adjustment between the four adjuster assemblies. The entire support frame is mounted on a linear rail system that translates the array 55 mm closer to the target centre from its nominal position or retracts it 700 mm further away from the nominal position in order to access the reaction chamber and provide additional space for detector installation and removal.

2.6.4 Array alignment

The flanges, shaft and base frame all have multiple laser tracking points to determine their exact location within the experimental hall's survey network, enabling them to be positioned accurately in relation to the target centre and PRISMA. Results from the simulations and tests demonstrated that the array, shaft and base frame are independently stiff structures, however the array deflects marginally at its interface with the shaft. When the array is constructed and individual flanges are mounted on the shaft, the gradual increase in load results in the array moving incrementally in relation to the shaft and survey network. In order to survey and align the array accurately during its assembly, these dynamic deflections must be negated. Consequently, the array is initially surveyed and aligned independently using the first flange mounted to the shaft as its datum from which the positional coordinates for subsequent flanges are referenced. By measuring the three reference points on each flange with the laser tracker, their position in relation to their true position (defined by the CAD model) can be determined, allowing them to be mounted with precision. Throughout the assembly process, mounted flanges are re-measured to ensure that the additional stress introduced into the array from the subsequent flanges have not altered their position. The final survey of the array's 81-point data set confirmed that the average positional error of the 27 flanges, without a slot, was less than 0.17 mm. Once the 30-flange array is assembled, their projected focal point onto the target plane, 1200 mm away, is measured. For the present set-up at LNL, each projected focal point onto the target plane is within 0.7 mm from the target centre, for the 27 flanges without a slot, see Fig. 11. After the average focal point of all the flanges has been determined, the overall structure is adjusted to position this on to the true target centre.

2.6.5 Cable and LN_2 hose management

Signal, power supply and autofill cables run from the detectors, over the top of the shaft and into a bespoke cradle cable management system that rotates with the shaft, before routing to the top of the racks that host the front-end electronics and LVPS. Cables for the mechanics drive and control system are routed through a cable tray that runs underneath the rotating platform, before coupling to the controller unit in a

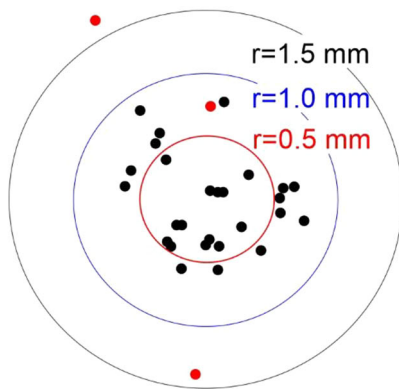


Fig. 11 Survey of the flange structure at LNL. The map is a projection of the focussing of each of the 30 flanges at the target position. The red dots correspond to the slotted flanges

second group of racks that host the HVPS system and autofill system.

The LN₂ is supplied from an external tank through a 40 m long transfer line into a long flexible hose that connects to a distribution manifold mounted on top of the flange array, before diverging to each detector.

2.6.6 Structural analysis

Finite element analysis (FEA) determined the probable deflection (see Fig. 12) and stress on the loaded structure. With the array loaded with all detector modules and the manifold mounted on top of the array, the analysis for the support shaft indicated that the shaft would deflect a maximum of -0.06 mm in the vertical Z axis and experience a maximum stress of 25 N/mm² from the estimated 40 kN maximum applied load.

The simulation for the loaded flange array (Fig. 13) demonstrated that the array itself would experience a maximum of -1 mm deflection in the Z axis, with the array pivot-

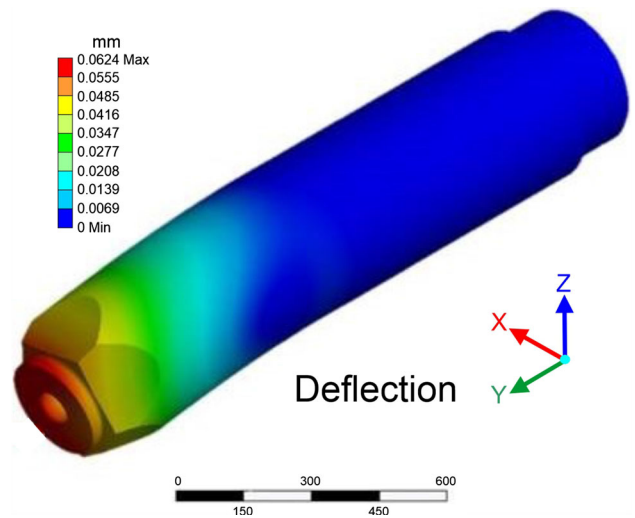


Fig. 12 FEA of the deflection (mm) of the loaded shaft

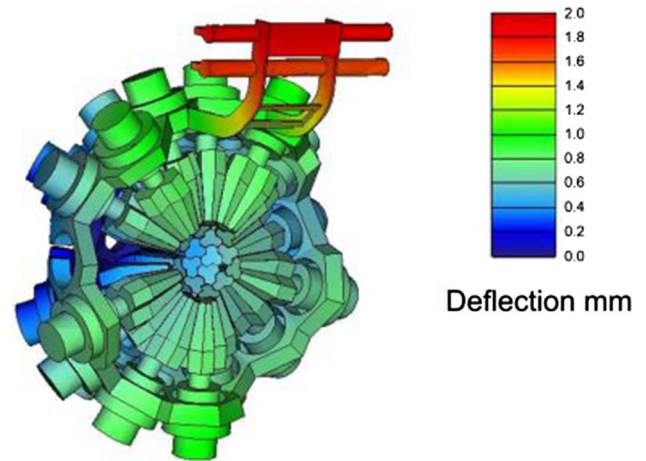


Fig. 13 FEA of the array, including the LN₂ manifold, mounted on the shaft, indicating deflection in mm

ing at its interface with the support shaft. The object furthest from the pivot, the manifold, experienced the largest deflection of -2 mm in the Z axis. The maximum stress of the setup at LNL is 60 N/mm² where the shaft connects to the flange array. The analysis included the impact of the array rotated at ± 85 degrees and determined that the offset load from the manifold and three unloaded flanges would not increase the stresses or deformations on the loaded structure. The support structure can accommodate ± 20 mm vertical adjustment, so alignment corrections from the deflections, determined by the analysis, are within the system’s capabilities.

When the array is rotated, the dynamic deflection of each module impacts the nominal 0.5 mm clearance between endcaps (Fig. 14). Due to their irregular shape and orientation, each module in the array encounters different forces, resulting in them experiencing a range of deflections. The analysis showed that endcap deflections ranged from 0.3 to 0.7 mm.

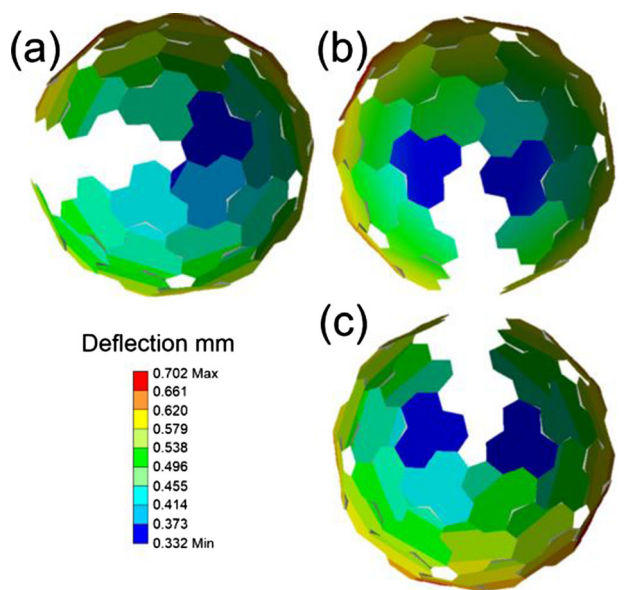


Fig. 14 FEA of the deflection (mm) of the endcaps with rotation of the array. **a** Normal position, **b** -90° and **c** 90° in experiment operation

However, the relative movement between neighbouring endcaps was no greater than 0.2 mm, indicating that the clearance between endcaps should be adequate for preventing modules coming into contact with each other whilst rotating the full array.

2.6.7 Physical testing

At Daresbury Laboratory in the UK, a series of physical tests were undertaken on the mechanical structure in order to validate the FEA and de-risk some of the assembly activities. These included an unbalanced load test that simulated only one-half of the array having modules mounted and a full load test that simulated the array fully populated with modules. A 1000 kg offset weight was mounted horizontally on the end of the shaft for 72 h to replicate the worst unbalanced load case. During this period, the encoder recorded an amount of displacement that was within the range attributed to the expansion and contraction of the structure due to diurnal temperature fluctuations in the test hall. Further tests with the offset load, demonstrated that the drive and control system was capable of rotating and holding the extreme offset load with precision. The full load test was carried out using 100 kg test weights mounted onto the array to represent the 30 detector modules and LN₂ manifold, see Fig. 15. The deflections of the system were measured using laser tracker and used to verify the FEA results.

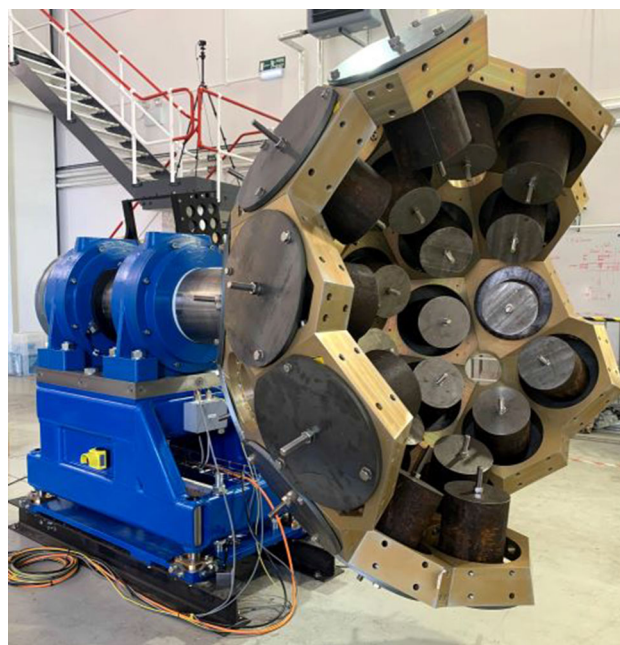


Fig. 15 Full load testing of the structure with dummy loads to replicate the weight of the modules and manifold

2.6.8 Rotation and control system

It is critical that the modules return to their original positions after the array has rotated to ensure that the data captured is consistent for every experiment. In addition, the fully loaded array must rotate in a smooth, controlled way to prevent the densely packed modules from flexing and coming into contact with each other due to excessive acceleration and deceleration forces. To provide AGATA with the required motion control and accuracy, its rotation is provided by a worm slew drive, driven by a StepSERVO integrated motor with a gearbox in-between the two. The dual gearbox design provides sufficient torque to drive the system with the precision needed whilst preventing back-driving when subjected to an unbalanced load. The shaft is coupled to a QCB WGWEA-17-104-25 HR slew drive with a 104:1 gear ratio, which in turn is driven by an inline stepper motor gearbox combination. Two Wittenstein gearboxes (SP140S at 10:1 and NP025 at 8:1) provide a combined ratio of 80:1 into the slew ring. The Applied Motion TXM34Q-5AG motor is a STEP Servo unit configured as a normal closed loop stepper that provides the system with a full operating speed of 0.1 RPM.

A Renishaw absolute optical encoder mounted on the bearing housing is used by the control system to track the rotational position of the shaft via the encoder scale fixed

radially to the shaft. The system is capable of positioning the array to within $\pm 50 \mu\text{m}$ of the required position. In addition to the software limits that restrict the array from moving beyond ± 85 degrees, mechanical limit switches have been fitted as a back-up, which safely stop the system at ± 86 degrees.

A simple physical interlock system helps prevent the array from being rotated accidentally as the shaft locking pin and interlock key for the drive controller are combined, so that the drive system cannot be powered if the pin is locking the shaft. The SM9903 control system is housed in a 19-inch rack 4U EMC enclosure. This contains a PM1000 motion controller with firmware that accommodates the 26 Bit BissC absolute encoder, which monitors the actual position of the load. The controller sends step and direction signals to the TXM34Q motor in response to commands from the supervising computer via the RS232 or a manual jog box. The encoder measures the shaft's rotation directly and this input is used to achieve its final position.

2.6.9 Triple detector module mounting and handling fixtures

For the 1π array, module mounting was achieved by driving the module mounting system onto the designated flange via three long rods. Two of the rods were temporary guide rods that were removed once the detector module had transitioned onto shorter linear bushings. A single threaded rod remained attached to the flange, which drove the module into position. To avoid damaging the modules on peripheral equipment during their insertion, long rods were used in previous campaigns to ensure that the module could maintain a steady trajectory into the array from a distance. Clearance around the larger 2π array is greatly reduced, so it is no longer feasible to use the long threaded rods to drive the modules onto the flanges, as these collide with the support platform and surrounding equipment. To maintain a long and controlled insertion path, modules are now inserted using a bespoke handling fixture that couples to the two short linear bushings. This fixture drives the module onto the linear bushes and a shorter threaded rod that translates the module to its final position, once the handling fixture is decoupled. The handling fixture translates the module via a hand-driven ballscrew and gearbox combination, which provides fine control and prevents the module moving under its own load (Fig. 16).

Whilst inserting the first module, it was discovered that it was not maintaining a steady trajectory into the array. The heavy module was driven horizontally into position using a single threaded rod and two sliding guide rods. Because of its weight and orientation, the module caused the insertion elements to deflect slightly, resulting in the module creeping backwards on the two sliding guide rods. This subsequent movement deviated the module from its ideal trajectory into

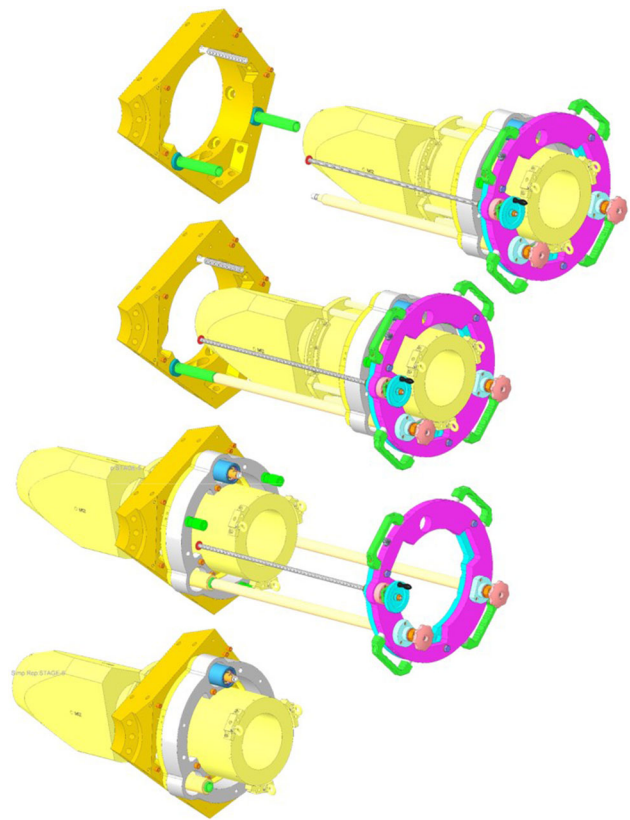


Fig. 16 Handling fixture coupled to a test flange with a replica triple detector module being inserted

the array. Threaded adjusters were retrofitted to the two short linear bushings, enabling the final and most critical phase of detector travel to be driven from three points instead of the one threaded rod (Fig. 17). This removed the unwanted pitching motion and improved the control of the module in the final phase of its insertion when endcap clearance is at its most critical. The handling fixture includes additional lifting points at specific locations to ensure that the modules are more evenly balanced when lifted and in the correct orientation for the corresponding flange. This system provides a controlled means of lifting, aligning and inserting each module into the array.

To help refine the handling process and reduce the risk of damaging the detectors, a replica triple detector module was fitted with accelerometers to record the forces it experiences during installation and removal. Using a dual ratchet hoist lifting system to control the pitch of the module and the handling fixture to provide a balanced lift, a handling procedure was developed that provided a safe and controlled means of inserting and removing the module. This enabled a single person to mount and dismount a detector module from ground level without it experiencing any event over 0.4g (Fig. 18).

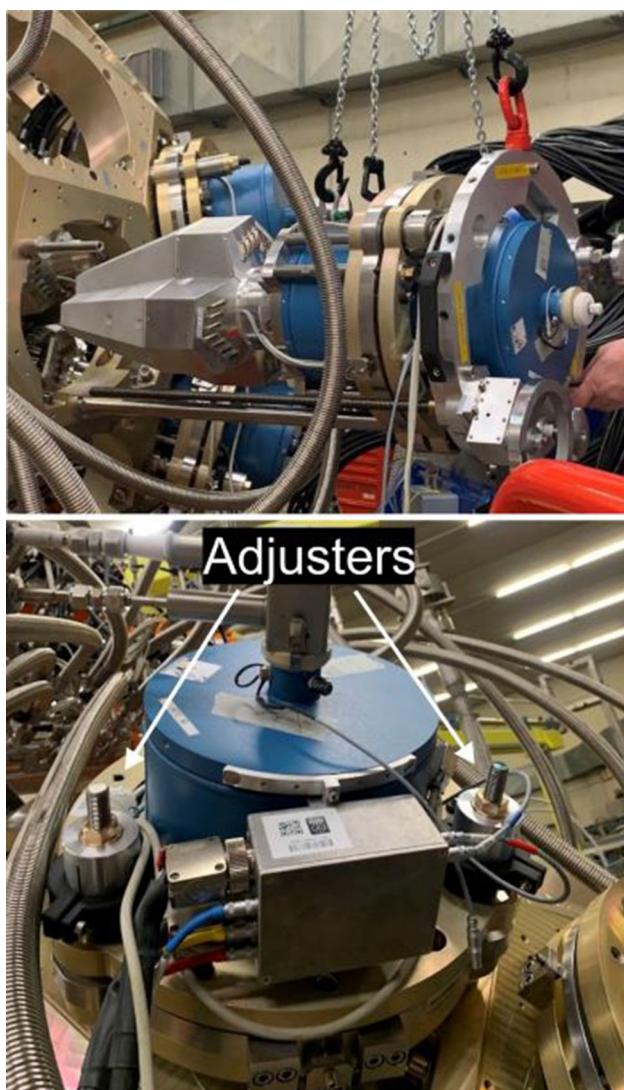


Fig. 17 Photographs of the triple detector module being mounted. The additional threaded adjusters are indicated in the bottom picture

2.6.10 Detector module survey tooling and alignment

The position of a detector module in relation to the target centre was previously established with a laser tracker capturing multiple points around the module's endcap by manually tracing a survey retroreflector around the endcap's edges. This difficult and time-consuming process had to be repeated each time a detector module was adjusted to record its new position. Once a neighbouring module was installed, the desired 0.5 mm clearance between endcaps made it impossible to accurately trace the opposing edges of the endcap with the retroreflector. Consequently, surrounding modules had to be partially withdrawn to allow sufficient clearance for the retroreflector to take measurements of the previously inaccessible edges. As a result, each module had to be retracted after they had been surveyed with the presumption that they would

Shock logger data

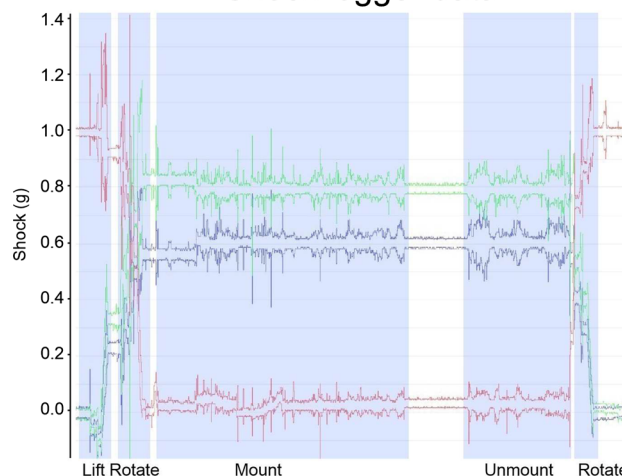


Fig. 18 The shock data measured during the lifting, rotating, mounting and unmounting of the triple detector module

return to their original location once reinserted. Given the challenges and risks associated with moving densely packed modules, this survey process, in the previous campaigns, was primarily reserved for the first five modules in the centre of the array.

To overcome these issues, two bespoke tools for surveying AGATA's modules were developed, an endcap survey tool that mounted onto the module's endcap and a dewar survey tool that fixed to the rear of the dewar, see Fig. 19. The lightweight aluminium endcap survey tool utilised the endcap's 3D model geometry to generate mating features that fitted squarely in a unique way on the surfaces of the endcap. Six thin metallic tabs on the tool's outer surfaces located it precisely on the outer faces of the endcap and allowed the tool to be temporarily secured to the endcap with KAPTON tape. The thickness of the stiff spring steel tabs is 0.2 mm, so they fitted between fully inserted modules and allowed the endcap survey tool to measure the final location of any module without retracting surrounding modules. The endcap survey tool utilised bonded magnetic nests that secured the metallic survey retroreflectors at four reference points. A single nest is situated on the module's central axis, whilst the others are located radially along each polygonal plane.

The exact location of the rear of the module is not as critical, so the dewar survey tool mounted from existing features on the fabricated dewar and utilised existing tapped holes to mount a tool with a single survey retro-reflector on the module's central axis. The dewar survey tool extended above the dewar's inlet feed, enabling it to remain fitted without restricting access to refill the dewar. Once the 3D printed prototypes had been refined and tested on working modules, the final tools were produced using precision manufacturing techniques in order to achieve the close tolerances needed

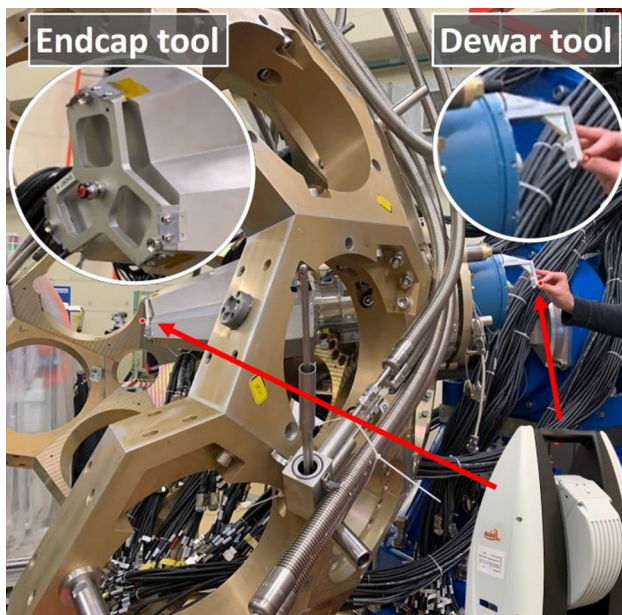


Fig. 19 Bespoke tools on the front and rear of the triple detector module for alignment using the laser tracker

to ensure the tools could achieve a precision fit. A repeatability test was conducted on the final endcap survey tool to ensure that it would perform as desired. Tests included the removal of the laser tracker targets from their nests and the removal of the tooling from an accurate replica of a module's endcap (Fig. 19). Over a 40-point data set, the average repeatability error was 0.022 mm, excluding internal errors of the laser tracker. Both tools provided five repeatable survey points on the module for the laser tracker to accurately measure and determine its location. In addition, the survey tooling allowed the module's endcap to be accurately tracked throughout its insertion into the array.

In conjunction, the two upgrades (endcap survey tool and driving the module from three points) now allowed the trajectory of each module to be accurately tracked and corrected throughout their entire journey into the array. This ultimately produced an average measured distance from the front faces of the ATCs to the target of 229.95 mm with an average displacement of 0.11 mm. This is an improvement compared with the previous installation at GANIL, where the average distance to the target was 230.9 mm with an average displacement of 0.4 mm. Furthermore, the module mounting time was reduced by a factor of two, compared with previous campaigns.

A photograph of the setup during the commissioning at LNL in 2022 with 11 triple detector modules, Fig. 20, shows the result of the accurate alignment of the ATCs.



Fig. 20 The array with 11 triple detector modules during commissioning of the spectrometer at LNL in 2022

3 Infrastructure upgrades towards the 4π array

The AGATA infrastructure consists of several items: the DSS, the database of all components and the proper grounding configuration. The DSS comprises hardware components, including the detector and digitiser LVPS, the autofill system for the Ge detectors, cables and patch boxes. It also has an integrated slow-control software to manage and supervise the detector operations, including Ge high voltage and temperature, autofill control, preamplifier and digitiser low voltage and uninterruptible power supply status. A database is necessary for the AGATA collaboration to build and maintain this complex array, keeping track of the details (such as characteristics, status, location) of several thousands components. An electromagnetic compatibility (EMC) characterisation of the installed components needs to be performed at each host laboratory in order to identify and eliminate weak grounding connections. It is an essential process to minimise the effects of external noise and optimise the detector performance.

After the initial installation at LNL in 2009, DSS components have been continually updated to comply with the evolving electronics production [16], from the initial version, V0, based on the ATCA standard [2], via the next version, V1, with computer-based GGP, to the present version, V2, based

on Ethernet communication. The DSS installed at GANIL [4] was sufficient for a setup with 15 ATCs, but it could not support the demands of the increasing number of detectors in the array.

For the new campaign at LNL, a simple incremental update was impracticable, as some items were obsolete or included discontinued components. Important upgrades were therefore necessary, which needed to be backward compatible and built with modern components, so that they can be easily produced in the future for the final configuration of 60 ATCs. The extension of the array to 2π , 30 ATCs, required the production of new LVPS crates and modules, an upgraded autofill system, the purchase and installation of a new HVPS, and the production and installation of additional sets of cables of the same kind as those developed and produced for the previous phase of the project [4].

The initial concept was to develop a modular DSS, scalable to the final 4π configuration and suitable for all host laboratories. Most adopted solutions meet these requirements. The autofill system cryogenic configuration is the only exception, as differences and constraints (e.g. safety rules, space) between host laboratories require some modifications. Great care was taken to optimise space and power consumption of the newly developed components and in all critical systems a fully remote control has been implemented.

Since the first campaign of AGATA at LNL, the integrity of the detector preamplifier signals was considered to be of the highest priority. There is a requirement to have the digitisers positioned within 10 m from the AGATA detectors to minimise the signal degradation (attenuation and integration) and this constraint strongly affected the development of mechanical systems and of several DSS components. The additional requirements to rotate and translate the detector array resulted in a complex cable management system to guide all cables to the electronics racks. All described systems are currently located on two extensions of the rotating platform supporting AGATA and the PRISMA spectrometer. The first extension, close to the AGATA mechanical support, has four racks housing all the digitisers of the front-end electronics and the LVPS units. The autofill system and HVPS are installed in two racks on the second extension close to PRISMA. A third rack on this extension hosts the front-end electronics for complementary detectors. Cable management between these two extensions is realised with a cable tray running underneath the rotating platform. Some key components of the overall layout at LNL are shown in Fig. 10.

3.1 High voltage, cables, detector patch boxes, low voltage, and optical fibres

3.1.1 High voltage

The HVPS that was used during the previous campaigns at LNL, GSI and GANIL was a CAEN SY527 system with CAEN A832 boards operated in the configuration that allowed the enabling of individual channels. These modules, previously used by the Euroball collaboration, are now discontinued and ongoing maintenance is not possible. Alternative replacement systems were tested at LNL and GANIL. All had similar datasheet specifications with improved current resolution and very low voltage ripple as compared with the older system. Moreover, they were equipped with control software and several communication interfaces (Ethernet, USB, RS232). Running servers, such as OPC, EPICS or Web services, allowed for their easy integration into more complex setups. For all tested systems, frequency spectra were equivalent to that obtained with the CAEN SY527 system, with no significant noise within the preamplifier-digitiser bandwidth. Marginal differences were observed at low frequency, without any significant effect on the Ge detector timing characteristics and energy resolution.

The CAEN HVPS system, based on the SY4527 mainframe with A1560H boards, meets the required performance, and the availability of high voltage boards with the control tools developed within the collaboration, made it the optimal solution.

3.1.2 Cables

In total, 29 cables are used for each ATC: three for high voltage bias, three for detector temperature and LN_2 level, two for low voltage and 21 for preamplifier signals. As indicated in Sect. 2.6.5, the cables run from each ATC into the cradle cable management system before being routed to the top of the racks that host the front-end electronics and LVPS. High voltage and Mini D Ribbon (MDR) cables directly connect the ATCs to the HVPS and digitisers. All other cables are connected to patch boxes installed on each ATC, see Sect. 3.1.3. Low voltage and MDR cables run to the LVPS and digitisers in the nearby racks, while high voltage and autofill cables are routed inside a cable tray underneath the rotating platform to the high voltage and autofill racks. Additional

service cables are used in the autofill system to read temperature and pressure sensors and actuate the valves. These run from the Programmable Logical Controller (PLC) modules over the top of the PRISMA spectrometer to the manifold installed above the flange array.

Whenever possible, to comply with stringent safety standards of the host laboratories, the installed cables are halogen free, flame retardant and low smoke with a jacket resistant against oil and hydrolysis.

Detector signals: The signals from each detector are transmitted to a digitiser using seven MDR cables. This solution has been selected after thorough investigation. Although all tested cables presented identical datasheet characteristics, only the Honda HTK EUROPE Ltd. cables were shown to preserve the signal integrity, in particular the fast rise time (about 100 ns), required to perform pulse-shape analysis [17].

High voltage bias: The Ge detectors are operated at bias voltage ranging from 4 to 5 kV. High-flexibility LSHF (Low Smoke Halogen Free) RG59 cables with SHV connectors and cable jacket materials that can withstand high temperatures are used.

Autofill: High-density multiwire cables are used to reduce the number of cables connecting the autofill system to the temperature and pressure sensors and valve actuators. Cables for the autofill system run from the PLC modules, over the top of the PRISMA spectrometer, to fan-out boxes that connect a single cable to eight individual lines. The boxes are mounted on top of the distribution manifold that rotates with the shaft.

Low voltage: The cables used to provide $-6\text{ V}/+6\text{ V}$ and $-12\text{ V}/+12\text{ V}$ bias for the ATC preamplifiers connect the LVPS, see Sect. 3.1.4, with the ATC patch boxes, see Sect. 3.1.3. For each ATC, two such cables are used, one for $+6\text{ V}/+12\text{ V}$ and the other one for $-6\text{ V}/-12\text{ V}$. In order to ensure a reliable performance in the sensitive and complex EMC environment and minimise the voltage drop over the cable length (15 m), a design was adopted consisting of six wire pairs (1.3 mm^2), shielded and twisted, with additional outer shielding. This solution provides the necessary characteristics, but results in a relatively rigid cable of 17 mm diameter.

The complex cable management needed, see Fig. 21, has been defined with simulations to ensure safe rotation and translation of the array, taking into account the unbalanced weight as well as the cable minimum bending radius and rigidity.

3.1.3 Detector patch box

Low voltage, PT100 and LN_2 level cables are connected to each ATC via a dedicated patch box (Fig. 22). The patch box provides a transition between the two input low voltage cables connected to the LVPS and the output individual power supply cables that are necessary for each of the three Ge detectors. Moreover, each patch box contains four passive



Fig. 21 Cable management system allowing for the array movements (rotation and translation)

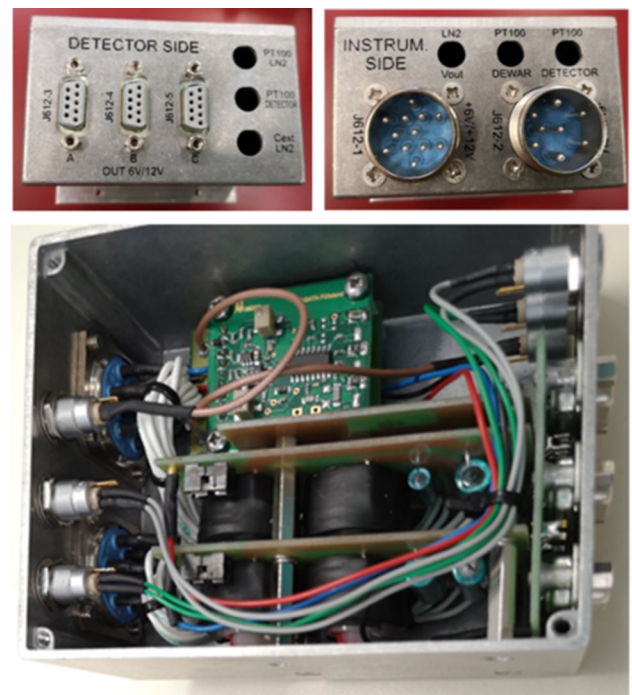


Fig. 22 Photographs of the metallic patch box showing the detector and electronics connections (top) and the internal components (bottom)

filters with different cutoff frequencies, installed on the $+6\text{ V}/+12\text{ V}$ and $-6\text{ V}/-12\text{ V}$ input power supply lines from the LVPS modules. A PCB with a conversion board (designed by IKP Cologne) is also included in order to monitor the LN_2 level inside each dewar.

3.1.4 Low voltage power supply

The original LVPS consisted of a + 48 V/+ 5 V module for the first-generation digitisers used in the AGATA setup (V0 electronics [2]) with power consumption of 480 W, the + 6 V/+ 12 V and –6 V/–12 V modules necessary to power the preamplifiers of the three Ge detectors integrated in an ATC as well as a +6.5 V module intended for an integrated HVPS. Remote control was available through a Profibus DP fieldbus interface. A single LVPS crate of 4U integrated all modules necessary for one ATC. Some LVPS units included an additional display for measuring output current and voltage.

To cope with the increasing number of detectors towards the 4π configuration, new digitisers (V1 [16]) were developed with a lower power consumption (≈ 120 W). Consequently, an important upgrade of the LVPS has been undertaken with the following characteristics:

- Be more compact;
- A revised + 48 V module compatible with power requirements of the V1 digitiser, as well as its new version V2 [16], currently under development (150 W);
- No changes to the + 6 V/+ 12 V and –6 V/–12 V modules for the preamplifiers;
- No changes to the Profibus DP fieldbus interface for remote control.

A reduction of volume and weight (as much as a factor of two for the former) was obtained by elimination of the unused + 6.5 V module, and by using switching mode power supplies for the 48 V modules, instead of the linear mode used in the first generation LVPS. The reliability of the new solution and the absence of any EMC disturbance in the system have been verified. The 48 V and 6/12 V LVPS units were placed in two separate crates of 8U each, each of them supplying eight ATCs. There is one Profibus controller for each crate, and the current and voltage readouts for individual channels are provided on the front display. Each of the 48 V outputs can be controlled individually, contrary to the previous version, where there was a single control for each ATC (three channels). The obtained space reduction is illustrated by the photograph in Fig. 23 that shows that the new unit supplying eight ATCs occupies a similar space as four first-generation units, with each of them connected to a single ATC.

A dedicated test bench was also developed to travel with the array to facilitate problem diagnostics.

3.1.5 Optical fibres

The V0 and V1 electronics relies on optical fibres for fast transfer of digitised signals to the pre-processing stage, and to the Global Trigger and Synchronisation (GTS) system. In both solutions the pre-processing computing farm is placed

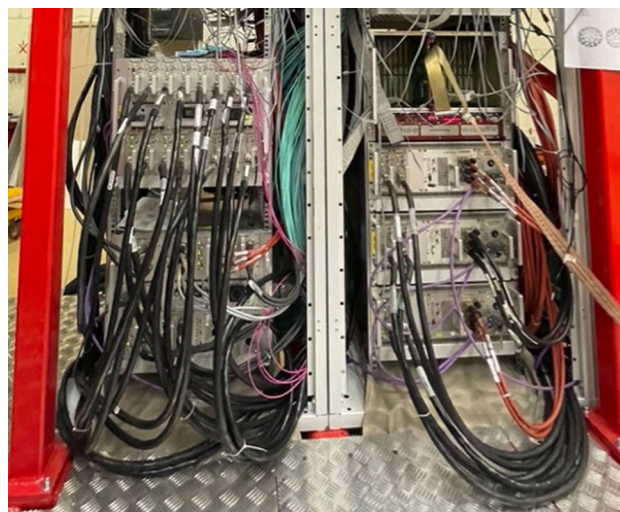


Fig. 23 Photograph of the LVPS systems installed at LNL showing three first-generation LVPS units, each supplying a single ATC, mounted in the rack on the right, and one new LVPS system for eight ATCs mounted in the rack on the left

in a different location with respect to the Front-End electronics (pre-amplifier + Digitiser) and the delay introduced by long optical links requires a careful selection of the hardware interface and precise signal synchronisation. In the new V2 electronics, the pre-processing electronics will be installed together with the digitiser boards and use predominantly copper input connection. After the campaign at GANIL, the original V0 electronics was phased out. The V1 electronics uses a reduced number of 60 m long fibres, identical to those used for the V0 electronics. Extensive tests have confirmed the possibility to couple several of these fibres up to a maximum length of 200 m with no signal degradation. The next generation electronics (V2) will use a smaller number of specific fibres with switch concentrators for Ethernet communication. These optical fibres are not directly compatible with those used for V0 and V1 electronics, but their adaptation is possible.

3.2 Autofill

The autofill is an assembly of industrial devices used for managing and monitoring the automatic cryogenic fillings of AGATA detectors. Such a system must be reliable, scalable with the number of detectors in the array, versatile in terms of sensor types and able to interact with the users. In order to keep the detectors cold, the control system ensures periodic LN₂ fillings as well as emergency fillings in case of a detector warming up.

An attempt to define a configuration of the cryogenic installation common for all laboratories hosting AGATA was unsuccessful due to large differences in the existing infrastructures of the host laboratories. An example is the use of

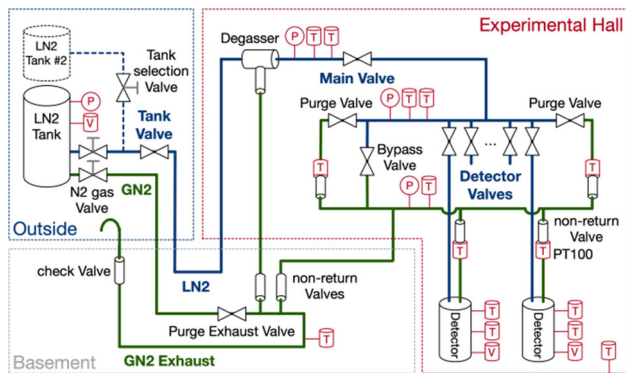


Fig. 24 Schematic layout of the cryogenic installation at LNL. The LN₂ level (V) and temperature (T) gauges, inside each detector cryostat, monitor the status of the detectors. The LN₂ level (V), pressure (P) and temperature (T) gauges in the external cryogenic reservoir, and along the LN₂ distribution line and manifolds, are used to control the filling cycle and for diagnostic purposes

direct filling from the main outside tank at LNL, while buffer tanks are needed at GSI, [3] and GANIL [4]. Consequently, the autofill system has to be flexible to facilitate these differences that are unavoidable when moving from one site to another.

At LNL, a 40 m LN₂ distribution line is used to connect an external LN₂ reservoir to the AGATA array. In the previous LNL campaign [1,2] the cooling of the entire distribution line was necessary at every filling cycle, taking about 30 min before detector dewars could be filled. The use of buffer tanks in the GSI [3] and GANIL [4] campaigns reduced this time considerably. The cryogenic architecture for the present setup at LNL, presented in Fig. 24, includes a gas separator (degasser) and optimises the position of the control valve to get an effective transfer LN₂ line shorter than 5 m, which minimises the time necessary for the LN₂ to reach each detector cryostat. Moreover, to improve the system reliability and reduce risk of water condensation close to the detectors, the entire LN₂ distribution system is isolated in vacuum, including the metallic flexible hoses connecting the LN₂ manifold with each ATC. An exhaust line at atmospheric pressure guarantees a correct evacuation of the N₂ liquid/gas produced during the filling cycle outside the building. N₂ gas (at room temperature) from the external reservoir is injected into the exhaust line to speed-up the evaporation of residual LN₂ and the line evacuation. Non-return valves are used to prevent backflow of N₂ liquid/gas to the detector cryostats and the buildup of pressure inside the manifolds. With this configuration, the estimated LN₂ consumption for the 2 π array of 90 detectors at LNL will be ≈ 1000 l/day.

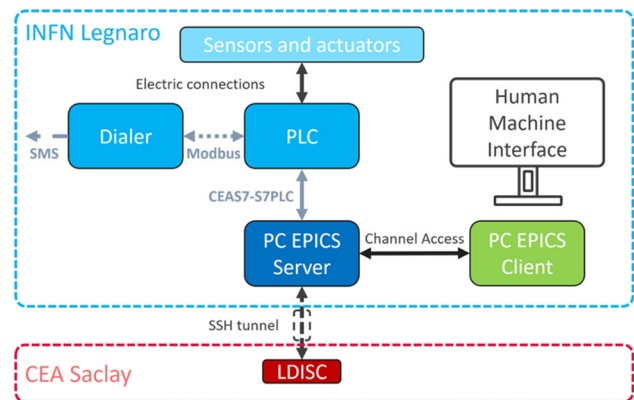


Fig. 25 Schematic layout autofill control architecture

3.2.1 Autofill control architecture

The present control system is composed of blocks of standard elements, with each block controlling 16 detectors. The elements are Siemens PLC cards managing temperature and pressure sensors as well as valve actuators. A Siemens PLC Central Processing Unit can communicate with up to four blocks. For the 2 π AGATA configuration at LNL only two blocks are used. Cryogenic and security processes are managed in the PLC Central Processing Unit (CPU), which also communicates with the alarm system (dialer) and the EPICS server, as illustrated schematically in Fig. 25. LDISC is the Saclay local EPICS PC, necessary to have direct access to the LNL EPICS server. The sensors read out by the system are 2-wire and 4-wire PT100 for temperatures, 4–20 mA sensor for pressure and 0–10 V signal for LN₂ levels. Valves are managed in two ways: 4–20 mA for regulation and 0–24 V for digital control. All modules, with an exception of the dialer, are located in two EMC racks dedicated to cryogenic control and HVPS.

EPICS Graphical User Interface (GUI) allows operators to interact with the control system, i.e. initiate sequences of operations, select LN₂ dewars to be filled, control LVPS, check alarms and define thresholds.

3.2.2 Autofill functions

Automatic filling: Automatic cryogenic filling of detector dewars is the main function of the autofill. This includes both regular fillings, when detector temperatures remain below a user-defined threshold, and forced fillings in case of a detector warming up. In this case, the high voltage of the affected Ge detector also needs to be shut down. PLC decisions are based on the dewar PT100, and a second PT100 (installed on the Ge detector) as well as the LN₂ capacity readout are monitored by the system. The autofill system response time after

a detector filling request is about two minutes. Four detector dewars can be filled at the same time.

EPICS GUI and archiving: An EPICS GUI enables operators to communicate with the autofill. It provides views for each aspect of the control, which includes feedback from the sensors and commands that can be sent to the actuators. A remote EPICS interface is available on the LNL network for local and remote control. Data are saved on the EPICS server and can be visualised on dynamic dashboards locally developed using the Grafana open source analytics and monitoring platform.

Low voltage power supply control: LVPS units are controlled by the autofill PLC using the Profibus industrial fieldbus. This communication allows operators to start and stop LVPS units via EPICS, as well as obtain information about their status.

Automatic restart: Following a loss of power to the racks, every component of the autofill has to restart automatically. For the electric part an auto-restart relay was integrated, and the EPICS PC and PLC restart automatically.

Remote connection: Remote connection to the autofill is possible through a dedicated VPN that enables communication with the autofill PLC and EPICS PC for updates, quick debugging and easy maintenance.

3.3 Electromagnetic compatibility (EMC) characterisation

The EMC characterisation is fundamental to guarantee the integrity of the signal while it travels from a Ge detector through the preamplifier (cold FET transistor and warm part) to a digitiser through a double-shielded MDR cable. To preserve the detector electronic performance, in the present configuration the entire AGATA setup (mechanical structure and electronics) shares a common grounding, which is well separated from the other laboratory instrumentation. The quality of the AGATA EMC has been validated for both the basic mechanical structure (without detectors, power supplies and electronics) and the fully mounted setup, to ensure that all electronic equipment has a good grounding connection.

Three types of tests were performed, as described in the following, in order to verify the low- and high-frequency system response as well as the quality of the cable shielding.

3.3.1 Low-frequency response: ohmic part (4-wire measurements)

As the first step, the ground connection between the different components of the mechanical structure has been verified and improved. This was achieved through 4-wire resistance measurements, which provides accurate information on the resistivity between different elements of a complex structure. A schematic layout of the measurement setup is presented in Fig. 26.

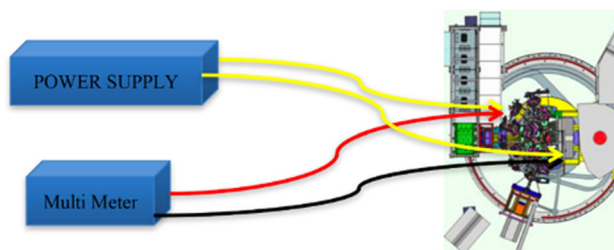


Fig. 26 Scheme of the 4-wire resistance measurements

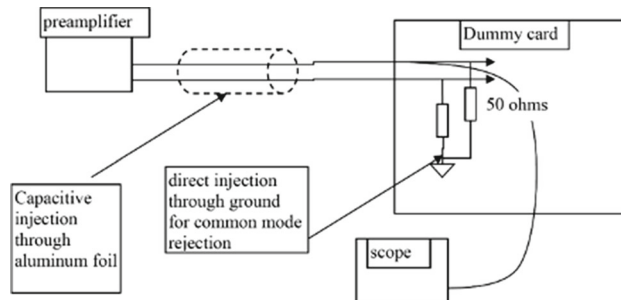


Fig. 27 Block diagram of the direct injection and capacitive coupling EMC measurements

First, a reference measurement was performed between two neighbouring points, one of them used as the origin for all following measurements. Subsequently, a current of 5 A was injected in various positions of the mechanical structure to determine the ohmic resistance with respect to the origin.

More than 70 points in the array structure were sampled. Most measured values are acceptable (below 5 milliohms). Few critical points above 25 milliohms and above 1 ohm (considered as open circuit) identified along the cable tray structure and racks, were improved by removing the paint on certain contact areas and installing a copper mesh over the entire length of the trays, fixed with several screws to the mechanical structure.

Ground connections to other equipment installed close to the array were also verified to minimise the impact of external noise and ground loops. As an example, a large resistance was measured on the beam line: an expected result, since the beam line and the array should not share a common grounding.

3.3.2 High-frequency response: direct injection to the ground

The direct injection method measures the common mode rejection ratio. The goal is to measure the voltage drop between two ground points when a high voltage fast transient pulse is injected in one of them, as shown in Fig. 27. The two points were chosen to be at least a few metres apart in order to calculate the impedance between them.

Imperfect connections are typically observed at mechanical junctions. For optimal electrical connection, larger contact areas must be free of paint.

The direct injection tests were performed after fixing most of the issues observed during the 4-wire resistance measurements. About 90 points in the array structure were considered. A scope was installed in the test point area, well shielded from other array components. A high voltage pulser injected a short 4 kV input pulse (5 ns rise time and 50 ns duration at half-amplitude) on the reference point. Large attenuation values, or correspondingly small signal-to-noise ratios ($\text{SNR} = 20 \log(V_{\text{measured}}/V_{\text{injected}})$), are characteristic of well connected components. For most tested points, excellent results were obtained (measured SNR lower than -95 dB). However, some grounding problems were diagnosed, which the previous 4-wire resistance tests were not sensitive to. Consequently, another metallic mesh with a sufficient contact area has been installed between each rack holding the front end electronics and different parts of the mechanical structure to optimise the grounding. As illustrated in Fig. 28, the adopted solution completely modified the grounding characteristics of the electronics racks: from the poor contact observed in the initial measurements ($\text{SNR} = -84$ dB) to the excellent result ($\text{SNR} = -102$ dB) obtained with the final configuration.

3.3.3 Cable shielding quality: capacitive coupling on the MDR cable shield

The capacitive injection measures the effect of a magnetic field on the cable ground shield. A high voltage Fast Transient Pulse (FTP) is applied to an aluminium foil, which is mounted externally on one extremity of the cable, as shown in Fig. 27. The voltage is measured on the preamplifier signal on the other extremity of the cable. This measurement shows the voltage drop caused by the FTP electromagnetic field generated inside the MDR cable. The cable shielding plays an important role to reduce this drop effect. The cable trays also play a crucial role: they should be metallic with the cables in a close contact with the metallic structure. If plastic or PVC trays are used (for example when flexible trays are needed) it is important to add metallic foils on the tray under the cables, grounding them on both sides.

All issues were solved and the 4 kV signal injected into the MDR cable shields resulted in a SNR always lower than -60 dB, with a negligible effect on the detector performance.

3.3.4 Final results

All components of the array have been developed to guarantee and preserve the detector performance. Thorough tests have confirmed that each of them fulfills the requested characteristics. However, interference effects could manifest in the detector signals after the assembly of the complex

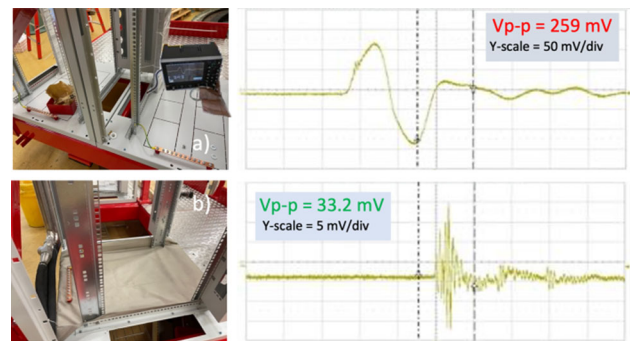


Fig. 28 Direct injection SNR measurements. After the installation of the electronics racks (a), the voltage (peak to peak value) measured at the vertical element was 259 mV ($\text{SNR} = -84$ dB). The measured voltage dropped to 33.2 mV ($\text{SNR} = -102$ dB), which corresponds to a very good grounding connection, when a copper mesh was installed to connect the racks to adjacent metallic structures (b). Oscilloscope horizontal scale is 200 ns/div

mechanical and infrastructure components with the entire electronics chain and acquisition system. In addition to verifying the energy resolution and time signals of the ATC detectors, the electronics noise of the digitised signals was analysed by performing a discrete Fast Fourier Transformation (FFT) of the HPGe detector signals. Baseline only signals were acquired in long waveforms (sample length 10^5 bins = 1 ms) from triggerless acquired events in all installed detectors. The time-dependent signals were converted to the frequency domain by performing a discrete FFT. Low frequency noise (10–100 kHz) is responsible to degrade the baseline quality, limiting the obtainable energy resolution. Detector timing and performances of Pulse Shape Analysis (PSA) algorithms are mostly affected by noise at higher frequencies (> 1 MHz), where efficient signal filtering reduces its impact on the energy resolution. The results for the central contacts of one ATC are shown in Fig. 29 and compared with a reference measurement performed at LNL in 2010. In the frequency region where the measurements are most reliable, i.e. below 1 MHz, the HPGe noise spectrum obtained with the current array is very close to the one measured in 2010 with a well controlled and much simpler configuration. Previously observed broader peaks within the preamplifier-digitiser bandwidth are not present. The reference spectrum taken at LNL in a cleaner configuration is significantly better only at low frequencies. An increased noise was observed only around 10 kHz, at the lower boundary of the preamplifiers working bandwidth. Several narrow peaks, associated to frequencies generated by specific components do not contain significant power. The very narrow peaks in the frequency spectra (one channel wide) are artefacts generated by the FFT algorithm. No effect on the HPGe energy resolution is observed.

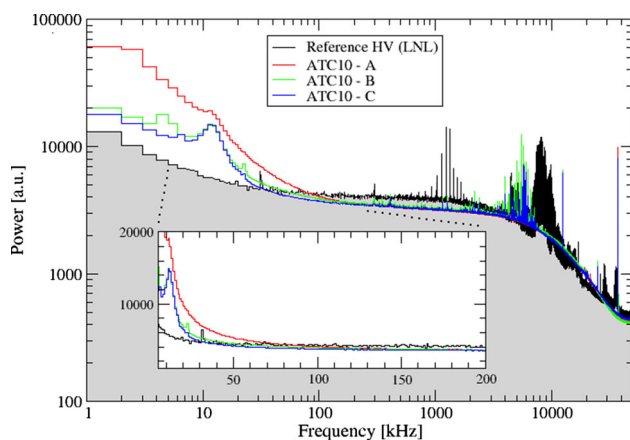


Fig. 29 FFT of HPGe baseline signals (sample length $10^5 = 1$ ms) for the three central contacts of ATC10 installed in the array together with 11 other fully operational ATCs (red spectrum—detector A, green—B, blue—C). In black, results of a reference measurement performed at LNL in 2010 are presented. Double logarithmic scale is used (double linear in the inset, showing the relevant frequency region for the baseline determination). The measurements are not sensitive for frequencies > 1 MHz and have a lower threshold at 1 kHz. The ATC10 spectra are normalised for a quantitative comparison

3.4 AGATA database and related tools

The AGATA Array Database (AADB) contains information on the current configuration of the array and keeps a record of its modifications. The AADB has been of fundamental help during the moves of AGATA between host sites. Moreover, it makes it easier to keep track of the unused, but still operational material that represents an AGATA legacy that can be loaned to other collaborations.

In view of such a long period of exploitation, a robust solution has been set up for the AADB. It relies on a SQL Oracle database hosted at CCIN2P3 (Computing Centre of IN2P3), which guarantees almost an uninterrupted service and regular and automatic backups to avoid loss of data. The scheme of the SQL database is complex, consistent and structured around the concept of generic objects characterised by three fields:

- A NAME that defines a global category for an object;
- A TYPE that defines a sub-category;
- A VERSION that allows to handle several versions of a particular object.

Individual objects are referenced by an attached unique alphanumeric bar code label. Additional information is indicated such as where the object is located, whether it is assembled or not inside another object, with the assembly rules being part of the database scheme to check for consistency. The SQL scheme has been designed so that it can be

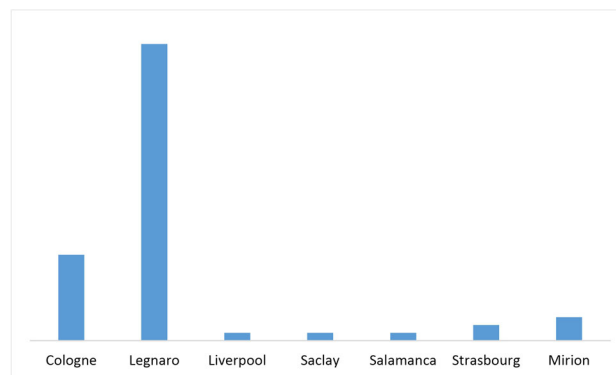


Fig. 30 Snapshot of the AADB on 16th November, 2022: location of the 56 AGATA Ge detectors at various collaboration sites as well as at the Mirion Technologies company

enhanced and be able to add specific information on specific objects.

Interactions with the AADB are performed through dedicated tools developed by the AGATA collaboration. A graphical user interface, called BigBrowser, written in Java, allows to perform many different standard actions such as registration of new objects, modification of assemblies, transport from one centre to another one, etc. This interface exists since the beginning of the project and is continually being improved to be as user friendly as possible, in particular for all the actions adding new records.

A recent development concerns the use of the AADB as a source of data. This approach has been implemented to allow building live dashboards from an internet browser. The full application, that contains a web server, has been containerised using docker technology. It runs on the kubernetes service available at CCIN2P3. From the web interface, users (access rights are managed by the application) can explore the database and build graphs, histograms and tables even without having to know the SQL language. The platform is also collaborative allowing to exchange part or full editable dashboards. It is possible to export underlying data sets into standard format (column-separated values, excel or json files).

As an example, Figs. 30 and 31 display two graphs directly produced by the web application. The first one provides information on the location of all the AGATA Ge detectors [8], which are distributed among the laboratories involved in detector characterisation, testing or maintenance (IKP Cologne, University of Liverpool, IRFU Saclay, University of Salamanca, IPHC Strasbourg), at the company Mirion Technologies for annealing or repairing, or (most of them) mounted on the array at LNL. The second graph gives the total number of computing nodes for the data acquisition (68) as well as information about the percentage still under warranty (34%), out of warranty (65%) and out of service (1%). The specific information for each computing node is available and allows to estimate the urgency of new purchases.

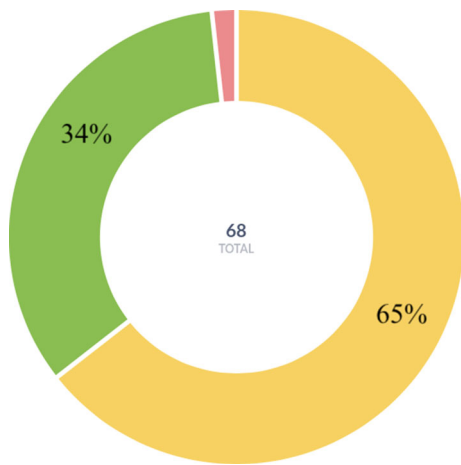


Fig. 31 Snapshot of the AADB on 16th November, 2022: warranty status of the AGATA computing servers. Green indicates servers under warranty, yellow those out of warranty, and red out of service

A similar information about the warranty status of each Ge detector is being inserted in the AADB.

New tools are under consideration such as applications for mobile devices based on the scanning of QR codes (or 1D bar codes) attached to the various components to keep the AADB up to date using modern communication technologies.

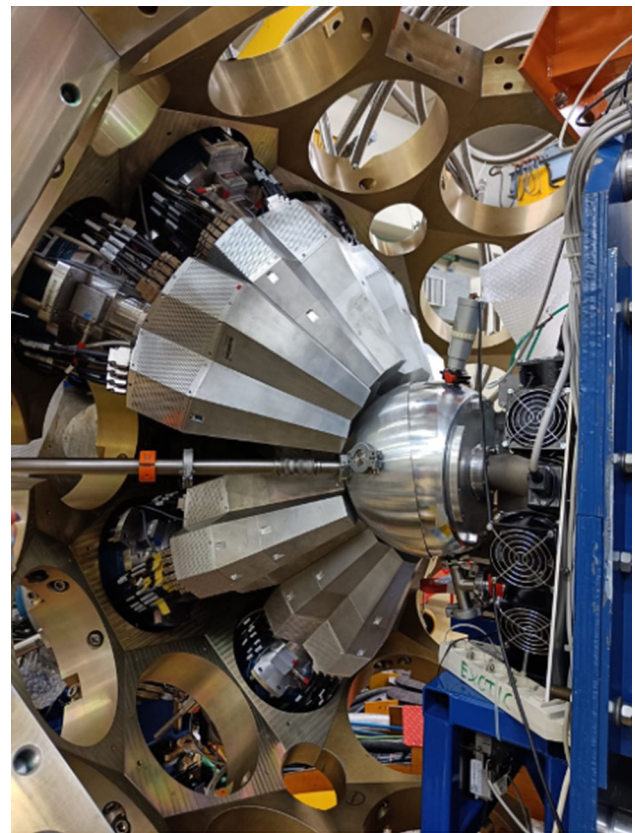


Fig. 33 AGATA setup in LNL with 11 ATCs placed around the reaction chamber, June 2022

4 Commissioning and installation

A panoramic view of the AGATA array including three ATCs during the installation phase (March 2022) at LNL with the

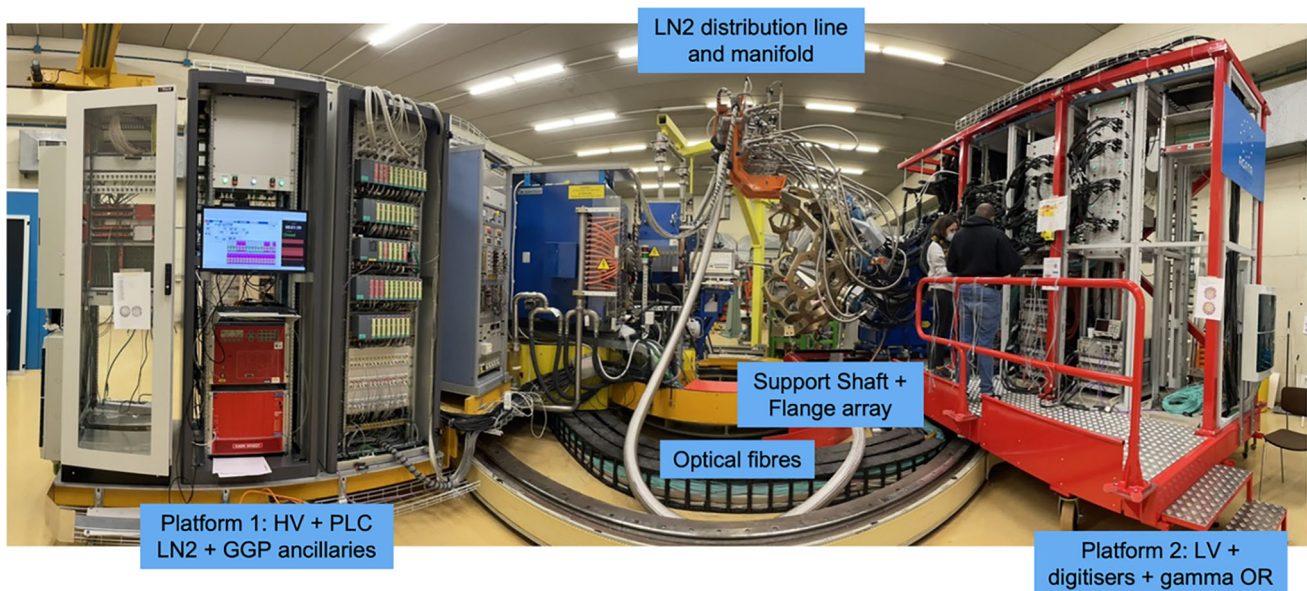


Fig. 32 General view of the AGATA array including three ATCs during the commissioning phase (March 2022). The main components of the mechanical structure and DSS are indicated

mechanical and infrastructure components described in this article is shown in Fig. 32. The setup with 11 ATCs placed around the reaction chamber used for the first experiments in this new campaign is shown in Fig. 33.

5 Summary

Mechanical structures and the DSS with all associated infrastructure including system services, with different constraints and properties, were successfully designed and implemented for the AGATA experimental campaigns at LNL, GSI and GANIL. For the present campaign at LNL many aspects have been redesigned and improved to realise a 2π spectrometer of up to 90 detectors [18]. AGATA has started its first science campaign at LNL in the new phase of the project, which is to increase the number of detectors to 180; the complete 4π spectrometer. The mechanics and detector infrastructures will remain a crucial part of this endeavour and the continuing scientific success of AGATA.

Acknowledgements The realisation of the mechanics, the DSS and associated infrastructures for AGATA is the result of a tremendous amount of hard work of a huge number of people in many laboratories. Particular thanks go to the skilled engineering and technical staff at the host laboratories and the whole AGATA collaboration. The contribution of the INFN groups from Legnaro, Padova and Milano, the CEA groups from IRFU/DIS and IRFU/DEDIP, the IN2P3 groups at IP2I and IJCLab, and the groups from Daresbury Laboratory is gratefully acknowledged. This work is funded in part by grants from the UK Science and Technology Facilities Council, including ST/F004052/1.

Data access statement Data sharing is not applicable to this article as no datasets were generated or analysed during this study.

Open Access This article is licensed under a Creative Commons Attribution 4.0 International License, which permits use, sharing, adaptation, distribution and reproduction in any medium or format, as long as you give appropriate credit to the original author(s) and the source, provide a link to the Creative Commons licence, and indicate if changes were made. The images or other third party material in this article are included in the article's Creative Commons licence, unless indicated otherwise in a credit line to the material. If material is not included in the article's Creative Commons licence and your intended use is not permitted by statutory regulation or exceeds the permitted use, you will need to obtain permission directly from the copyright holder. To view a copy of this licence, visit <http://creativecommons.org/licenses/by/4.0/>.

References

1. A. Gadea et al., Nucl. Instrum. Methods Phys. Res. **A654**, 88 (2011). <https://doi.org/10.1016/j.nima.2011.06.004>
2. S. Akkoyun et al., Nucl. Instrum. Methods Phys. Res. **A668**, 26 (2012). <https://doi.org/10.1016/j.nima.2011.11.081>
3. N. Pietralla et al., EPJ Web Conf. **66**, 02083 (2014). <https://doi.org/10.1051/epjconf/20146602083>
4. E. Clément et al., Nucl. Instrum. Methods Phys. Res. **A855**, 1 (2017). <https://doi.org/10.1016/j.nima.2017.02.063>
5. S. Agostinelli et al., Nucl. Instrum. Methods Phys. Res. **A506**, 250 (2003). [https://doi.org/10.1016/S0168-9002\(03\)01368-8](https://doi.org/10.1016/S0168-9002(03)01368-8)
6. E. Farnea, F. Recchia, D. Bazzacco, T. Kröll, Z. Podolyák, B. Quintana, A. Gadea, Nucl. Instrum. Methods Phys. Res. **A621**, 331 (2010). <https://doi.org/10.1016/j.nima.2010.04.043>
7. A. Wiens et al., Nucl. Instrum. Methods Phys. Res. **A618**, 223 (2010). <https://doi.org/10.1016/j.nima.2010.02.102>
8. J. Eberth, H. Hess, P. Reiter, S. Bertoldo, C. Carraro, G. Maggioni, D. R. Napoli, W. Raniero, D. De Salvador, AGATA detector technology, this Topical Issue
9. P. Fallon, A. Gade, I.-Y. Lee, Annu. Rev. Nucl. Part. Sci. **66**, 321 (2016). <https://doi.org/10.1146/annurev-nucl-102115-044834>
10. A.M. Stefanini et al., Nucl. Phys. A **701**, 217c–221c (2002). [https://doi.org/10.1016/S0375-9474\(01\)01578-0](https://doi.org/10.1016/S0375-9474(01)01578-0)
11. P. Golubev et al., Nucl. Instrum. Methods Phys. Res. A **723**, 55–66 (2013). <https://doi.org/10.1016/j.nima.2013.04.058>
12. A. Maj et al., Nucl. Phys. A **571**, 185–220 (1994). [https://doi.org/10.1016/0375-9474\(94\)90347-6](https://doi.org/10.1016/0375-9474(94)90347-6)
13. J. Eberth et al., Prog. Part. Nucl. Phys. **46**, 389–398 (2001). [https://doi.org/10.1016/S0146-6410\(01\)00145-4](https://doi.org/10.1016/S0146-6410(01)00145-4)
14. H.-J. Wollersheim et al., Nucl. Instrum. Methods Phys. Res. **A537**, 637 (2005). <https://doi.org/10.1016/j.nima.2004.08.072>
15. M. Rejmund et al., Nucl. Instrum. Methods Phys. Res. A **646**, 184–191 (2011). <https://doi.org/10.1016/j.nima.2011.05.007>
16. J. Collado et al., AGATA Front End Electronics, this Topical Issue
17. F.C.L. Crespi, F. Camera, O. Wieland, G. Benzoni, S. Brambilla, B. Million, D. Montanari, Nucl. Instrum. Methods Phys. Res. **A570**, 459 (2007). <https://doi.org/10.1016/j.nima.2006.10.003>
18. J.J. Valiente-Dobón et al., Nucl. Instrum. Methods Phys. Res. **A1049**, 168040 (2023). <https://doi.org/10.1016/j.nima.2023.168040>